Barcelona Supercomputing Center
Centro Nacional de Supercomputación

This poster is supported by the Joan Oró AGAUR-FI (2025 FI-1 00429) predoctoral grants program of the Department of Research and Universities of the Generalitat de Catalunya and co-financing by the European Social Fund.

A diagnostic package for the evaluation of key mean-state properties in climate predictions.

Ángel Sánchez-Lorente[1] , Pablo Ortega[1], Roberto Bilbao[1]

1. Barcelona Supercomputing Center, Earth Science Department, Plaça d'Eusebi Güell, 1-3, Les Corts, 08034 Barcelona, Spain. angel.sanchez@bsc.es

UPCLIV Workshop

reACT

MINISTERIO DE CIENCIA E INNOVACIÓN
UNIÓN EUROPEA Fondo Social Europeo El FSE invierte en tu futuro
AGENCIA ESTATAL DE INVESTIGACIÓN
Grant EUR2024-153543 was funded by MICIU/AEI/10.13039/501100011033 and by ERDF

1. INTRODUCTION

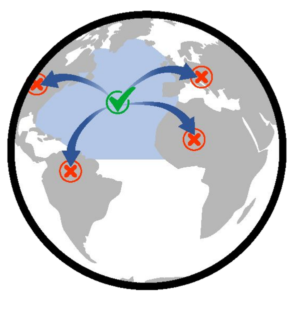

The ability of current forecast models to predict the atmospheric circulation, in regions like the **North Atlantic (NA)**, and through it the continental climate is undermined by a misrepresentation of key processes and interactions. In this work, we present a comprehensive suite of Python-based diagnostic metrics that measure the ability of climate prediction systems to represent those key underlying processes, including the influence of mesoscale eddies, atmospheric eddy feedbacks, and remote drivers of NA variability. This Python-based package will be used to guide the tuning of an eddy-resolving version of the last generation global coupled model IFS-NEMO specifically developed for climate prediction.

Methods

Models vs **Obs** → areas of interest
- Ocean
- NH Atmosphere
- Arctic ice

Data (DJF 1991-2020)

- **Models**: EC-Earth3 (ocean), SEAS5
- **Obs**: EN4 (ocean), ERA5, CMAP (precip)

2. NORTH ATLANTIC OCEAN

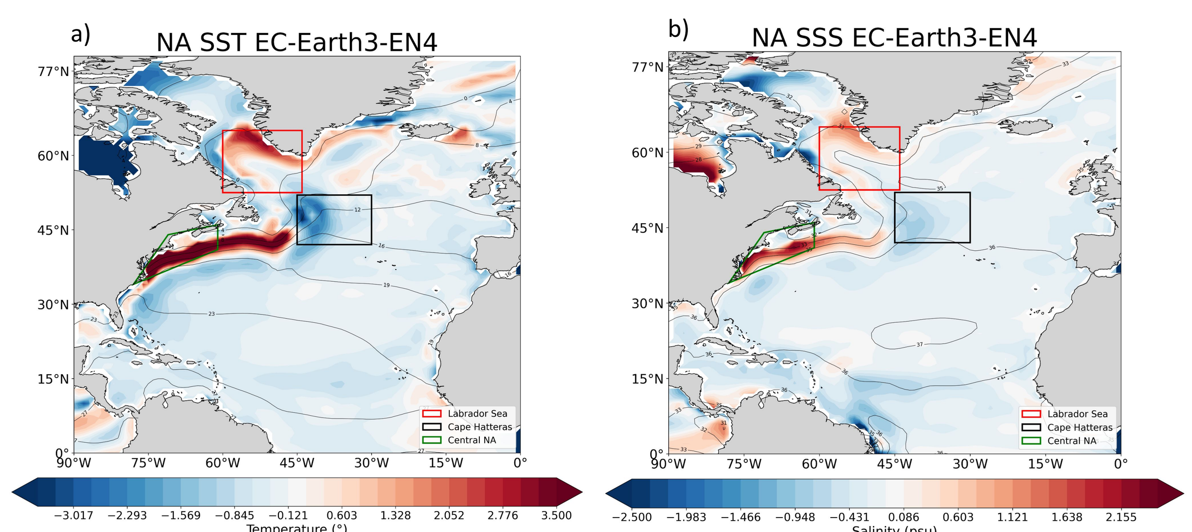

Figure (1): a) SST and b) SSS EC-Earth3- EN4 bias in NA, DJF 1991-2020. Red box, Labrador Sea (44–60 W, 52.5–65 N); black box (30–45W, 42–52N); green box Cape Hatteras (edges, (78 W, 34N), (61 W, 41 N), (61 W, 46 N), (71W, 44N). In contours, EN4 values.

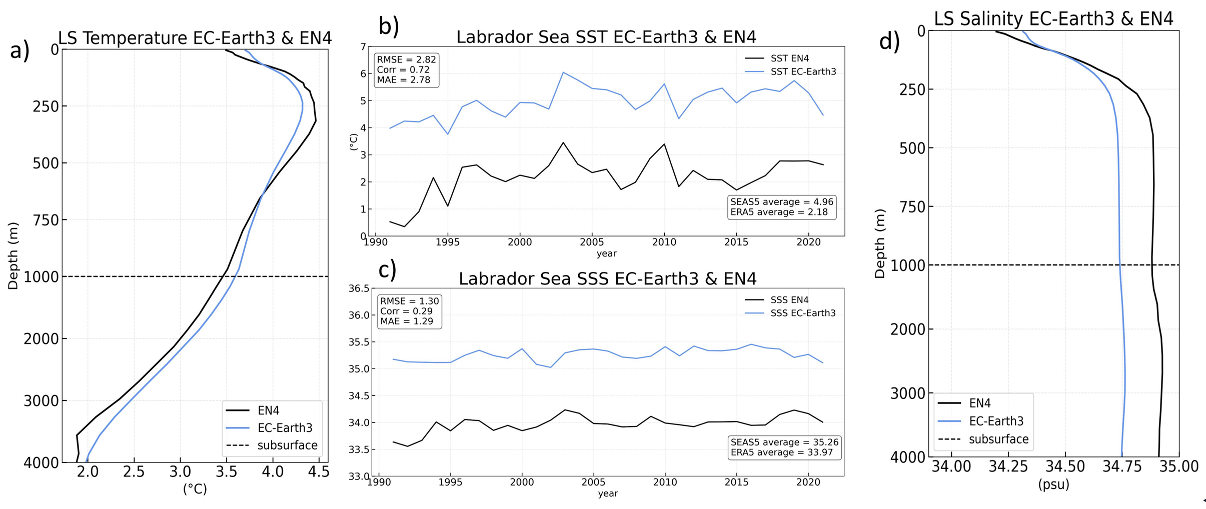

Figure (2): LS (red box in Fig.1) temperature and salinity fields for EC-Earth3 and EN4, DJF 1991-2020. a) and d), vertical profiles with zoom in the subsurface (black dashed line); b) and c), surface time series. In little boxes, statistical metrics: average, mean absolute error, Pearson correlation and bias.

The North Atlantic (NA) ocean is one of the main modulators of seasonal-to-decadal climate variability, influencing its neighboring continents. Biases in ocean salinity and temperature are good indicators of model shortcomings in representing key dynamical processes (e.g. the AMOC) and air-sea interactions (Frigola et al. 2025).

Processes of interest:
- Gulf stream strength and position
- Deep water formation in Labrador Sea
- Mesoscale eddy activity

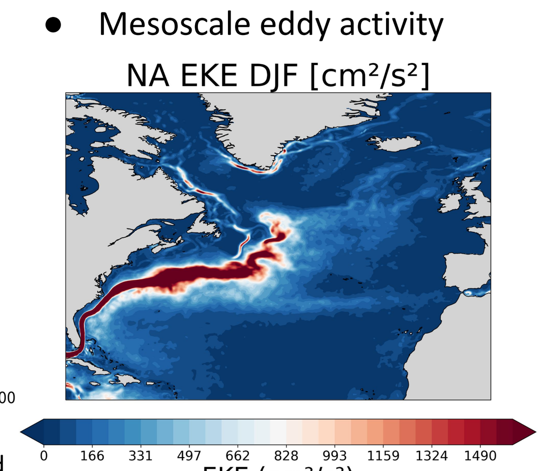

Figure (3): EKE (eq. 3) derived from satellite altimetry data, from Copernicus. DJF 1993-2020, daily data, preprocessed with a 10-30 day band-pass Butterworth filter.

3. TROPICAL PACIFIC

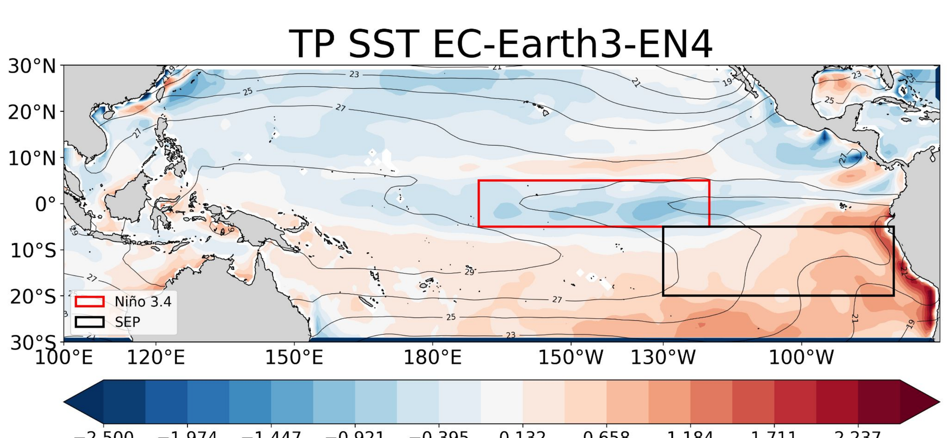

Figure (4): Tropical Pacific 1991-2020 DJF SST bias map (EC-Earth3 - EN4). Red box, El Niño 3.4 region [5S-5N; 170W-120W] (cold tongue); black box, southeastern Pacific region [5S-20S; 130W-80W] (warm bias). In contours, EN4.

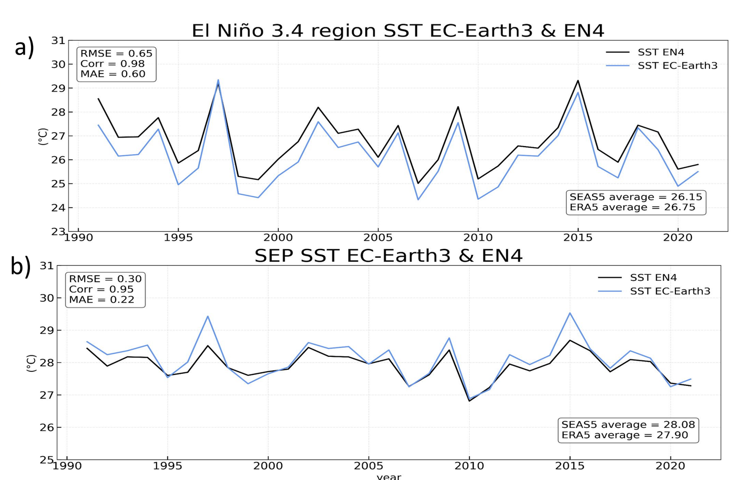

Figure (5): El Niño 3.4 (a) and SEP (b) time series, 1991-2020 DJF average; EC-Earth3 (blue) and EN4 (black).

Teleconnections

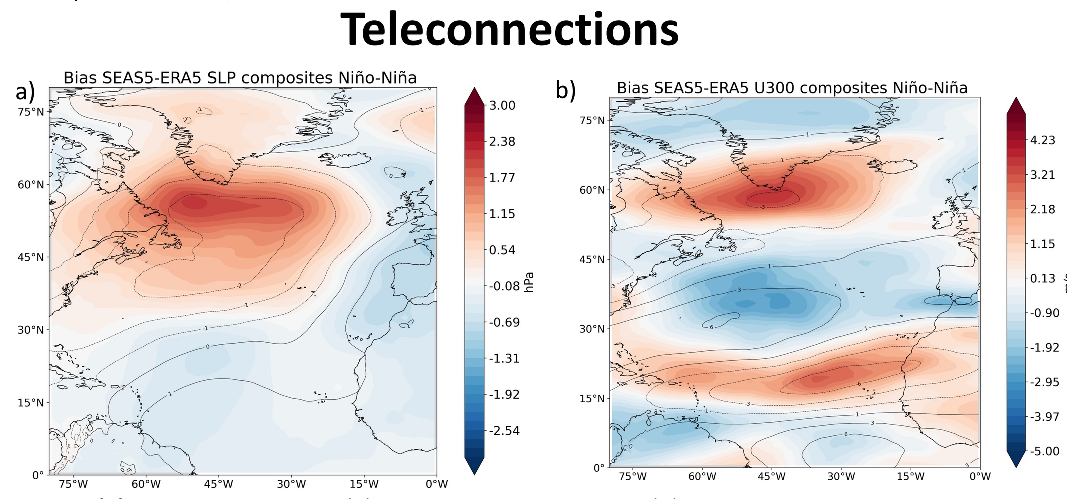

Figure (6): Sea level pressure (a) and U300hPa zonal wind (b) ENSO teleconnection difference between SEAS5 and ERA5 in NA sector. Teleconnection computed as the composite of the specific variable for Niño-Niña years. In contours, ERA5 values.

The Tropical Pacific is the core region of El Niño Southern Oscillation (ENSO), the principal source of seasonal predictability at global scales. Persistent model biases affect its mean state due to the complex local coupling between the ocean and the atmosphere (O'Reilly 2025).

Typical biases of interest:
- Cold tongue bias
- Doble ITCZ bias
- Southeastern Pacific warm bias
- Teleconnections in NA sector

4. DOBLE ITCZ

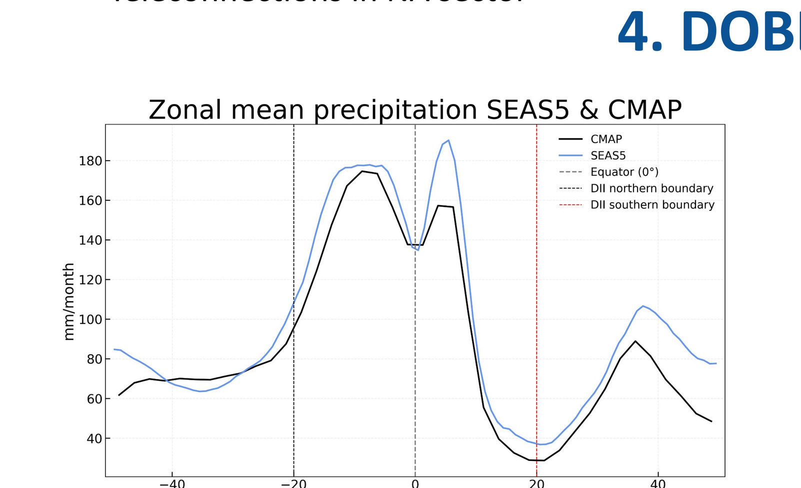

Figure (13): Zonally-average mean DJF precipitation/month, 1991-2020 for SEAS5 (blue) and CMAP (black). In black and red dashed lines, the thresholds for calculating the DII (see Figs 7 and 8)

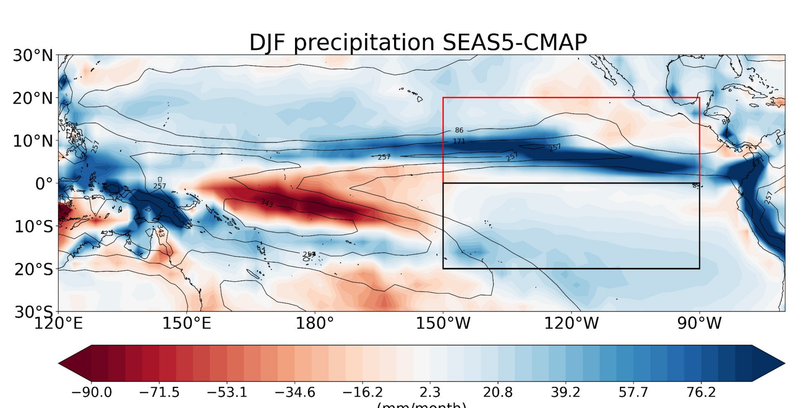

Figure (7): Mean DJF precipitation/month difference (SEAS5-ERA5) in Tropical Pacific, DJF 1991-2020. In red and black boxes, the regions used for calculating the DII in Fig. 8. In contours, CMAP values.

The double Intertropical convergence zone (ITCZ) bias is a common problem in current climate models. It is characterized by an overestimation of the southern branch of the ITCZ, most notably in the eastern Pacific (Dong et al. 2025). This issue is often reduced in high-resolution models.

Processes of interest:
- Double ITCZ index (DII, eq 1); precipitation asymmetry between tropical north and south hemispheres.
- SST in southeastern Pacific
- South America coastal cloud cover

$$DII = \frac{\overline{Pr}^N - \overline{Pr}^S}{\overline{Pr}^N + \overline{Pr}^S} \quad (1)$$

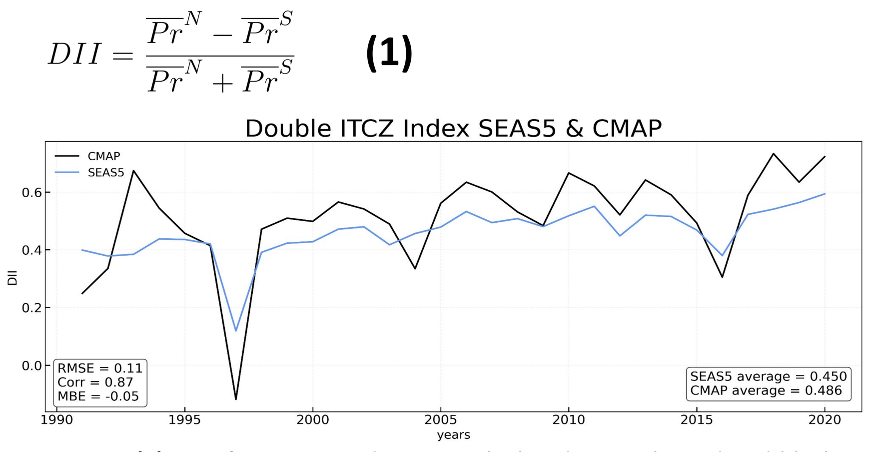

Figure (8): DII for SEAS5 and CMAP, calculated using the red and black boxes regions in Fig. 13. 1991-2021, DJF. Statistical metrics in white boxes.

5. STRATOSPHERE

Number of SSWs

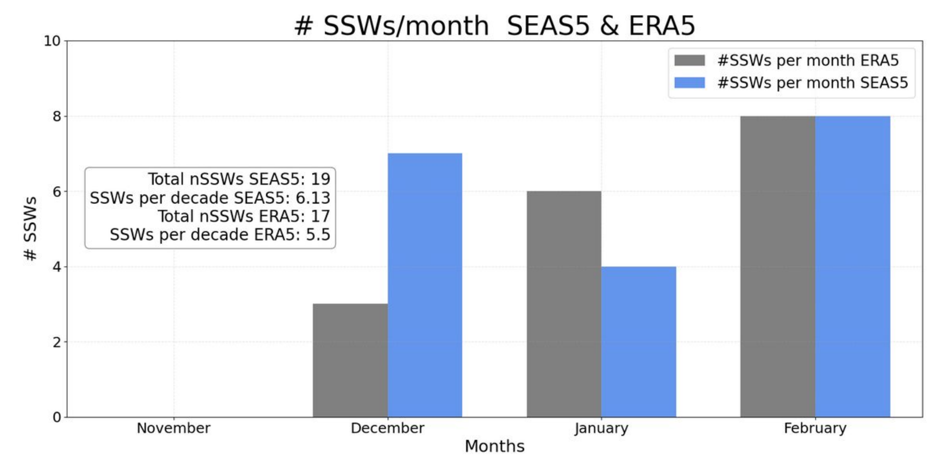

Figure (9): Number of SSWs per month. Period NDJF, 1991-2020. SEAS5 (blue) and ERA5 (grey).

The coupling between stratosphere and troposphere is of special interest for seasonal forecasting (Palmeiro et al. 2023). The maximum interaction between these layers takes place in the boreal winter, when upward Rossby waves interact with the Polar Vortex (PV). This interaction can lead to a weakening of the eastward stream of the PV, triggering sudden stratospheric warmings (SSWs), which are associated with (oftenly extreme) anomalous tropospheric circulation patterns modulating the surface climate up to several months in advance. Thus, a good representation of SSWs is of great relevance for enhancing climate predictability in winter in the high-latitudes of the Northern Hemisphere.

Processes of interest:
- PV strength and number of SSWs
- Stratosphere-troposphere coupling
- QBO teleconnections on the PV

Stratosphere-troposphere coupling

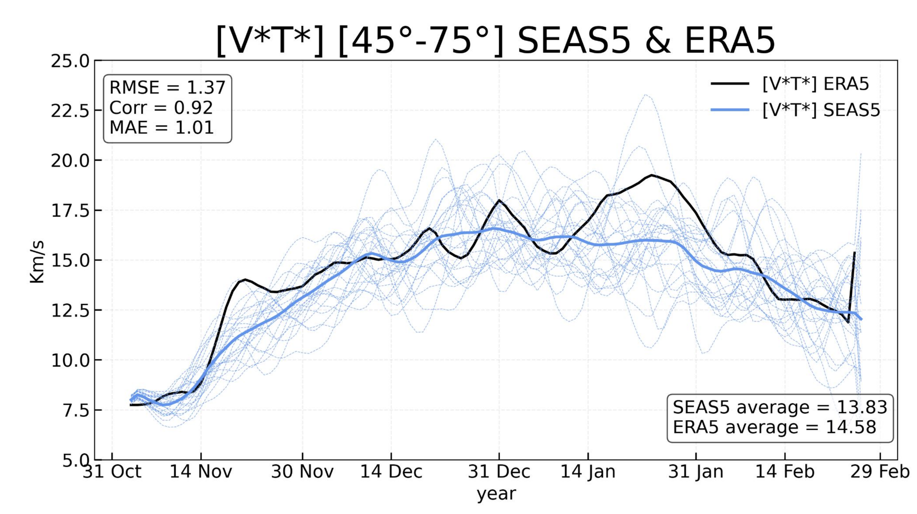

Figure (10): NDJF daily average wave activity measured as the zonally-averaged 100hPa eddy heat flux [V*T*] over 45-75N. 1991-2020 SEAS5 (blue, ensemble mean; dashed blue 25 members) and ERA5 (black). Statistics included in the inset boxes: root mean squared error (RMSE), Pearson correlation coefficient (Corr), mean absolute error (MAE), and winter average.

QBO teleconnection on the PV

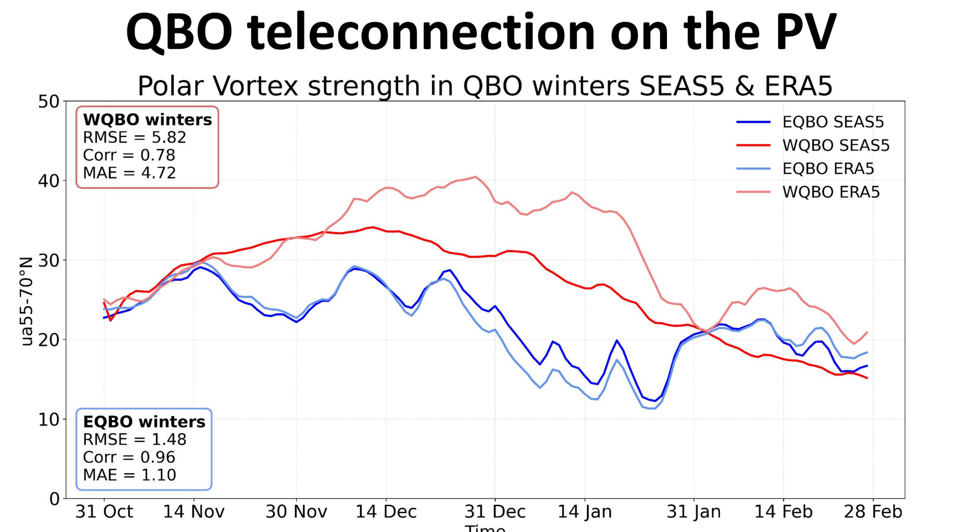

Figure (11): NDJF daily average QBO teleconnection composites on the PV, 1991-2020, SEAS5 & ERA5. PV strength defined as the ua10hPa [55-70N]. QBO phases: EQBO when ua10hPa [5S-5N]< -5m/s; WQBO, when >5m/s.

6. ATMOSPHERIC EDDY ACTIVITY

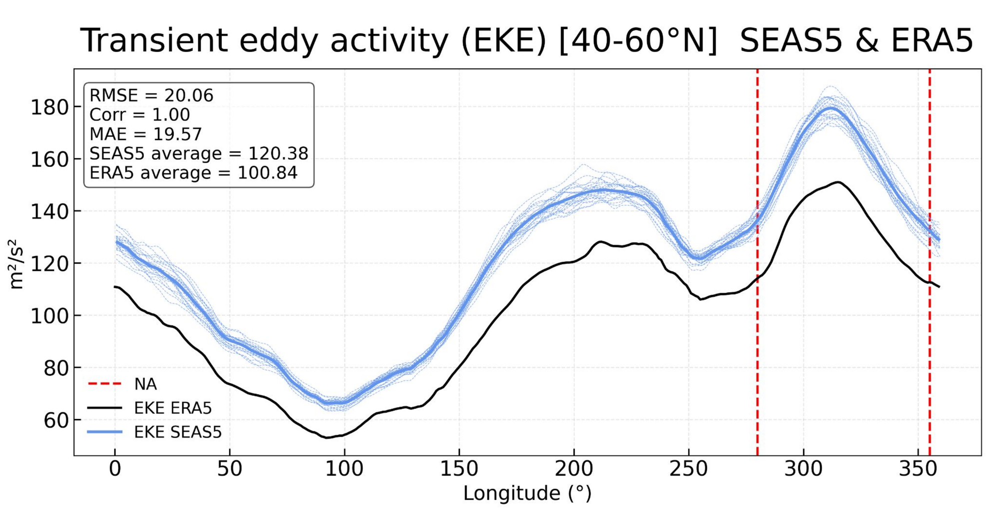

Figure (12): DJF North Hemisphere midlatitude-averaged transient eddy activity, 1991-2020, SEAS5 (blue, ensemble mean; dashed blue, 25 members) & ERA5 (black). Vertical red lines represent the NA sector. Statistical metrics included in upper-left box.

Mesoscale atmospheric processes and interactions are often misrepresented at standard model resolutions. This misrepresentation has been linked to the signal-to-noise problem in seasonal-to-decadal predicton. Thus, it is paramount to evaluate if the eddy activity and its interaction with the jet stream are well reproduced in the forecasting systems (Kang et al. 2011).

Processes of interest:
- Eddy feedback (eq. 2, 3): Correlation squared between zonal wind and the divergence of Eliassen-Palm flux, averaged over 500-300 hPa and 25°-72°N.
- Eddy Kinetic energy (eq. 4, EKE), preprocessed with a 2-10 days band-pass Butterworth filter.

Zonal mean QG momentum eq.

$$\frac{\partial \bar{u}}{\partial t} = f\bar{v}^* + \frac{1}{a\cos\phi}\nabla\cdot\boldsymbol{F} + \bar{\epsilon} \quad (2)$$

EP flux divergence eq.

$$\nabla\cdot\boldsymbol{F} = \nabla_\phi F_\phi + \nabla_p F_p = \frac{1}{a\cos\phi}\frac{\partial F_\phi \cos\phi}{\partial\phi} + \frac{\partial F_p}{\partial p} \quad (3)$$

$$\mathrm{EKE} = \frac{1}{2}\overline{(u'^2 + v'^2)} \quad (4)$$

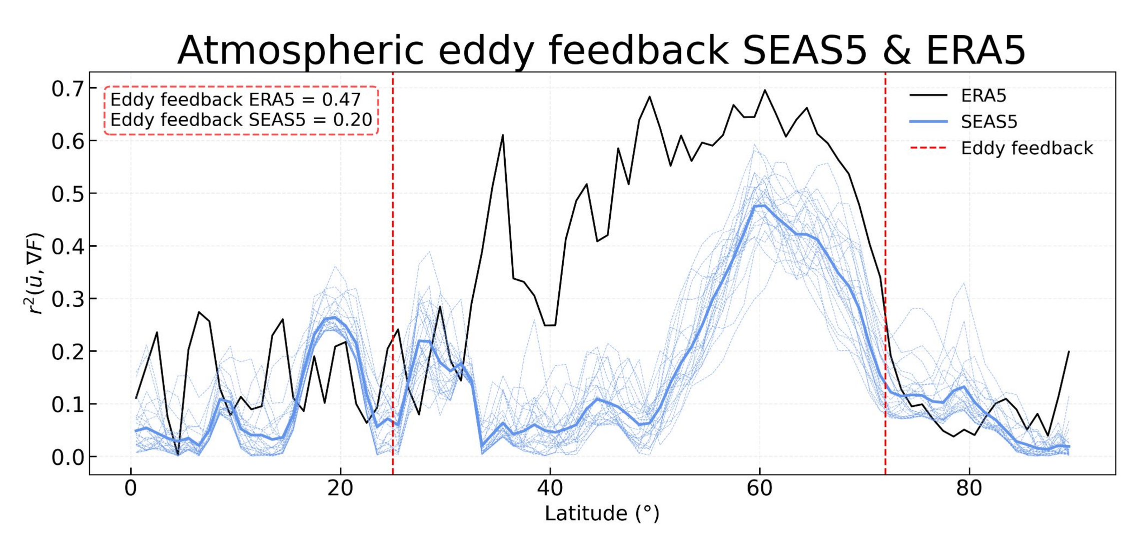

Figure (13): DJF North Hemisphere zonally-averaged atmospheric eddy feedback, 1991-2020, SEAS5 (blue, ensemble mean; dashed blue, 25 members) & ERA5 (black). Vertical red lines represent the latitudes where the eddy feedback parameter (upper-left red dashed box) is computed.

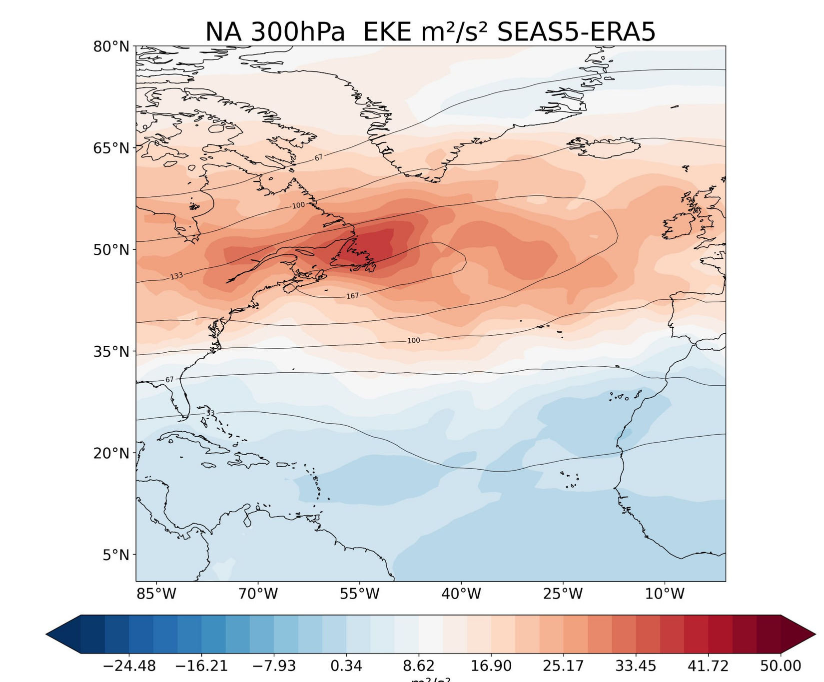

Figure (14): Difference in 300hPa transient eddy activity between SEAS5 and ERA5 (shaded) in the NA sector (red dashed box in Fig.12), DJF 1991-2020. The contours are the ERA5 values.

7. ARCTIC

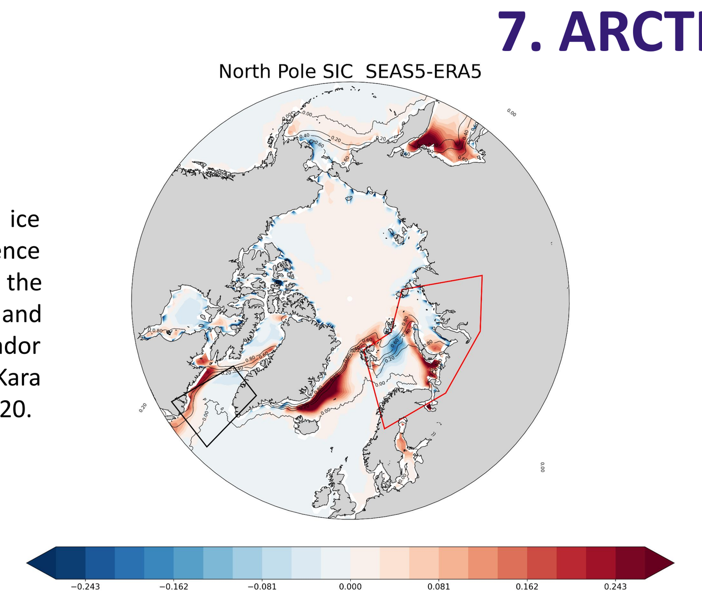

Figure (15): DJF Sea ice concentration difference (SEAS5 - ERA5) in the North Pole. In Black and red boxes, the Labrador Sea and Barents-Kara Sea regions. 1991-2020.

We focus on two main regions for their link with the atmospheric and oceanic circulation in the NA sector (Acosta-Navarro et al. 2020):

- **Barents-Kara Sea:** driver of North Atlantic Oscillation (NAO) variability, mid latitude tropospheric and stratospheric dynamics.
- **Labrador Sea**: modulator of deep water formation in the North Atlantic. Sea ice biases can hinder the representation of deep water mixing.

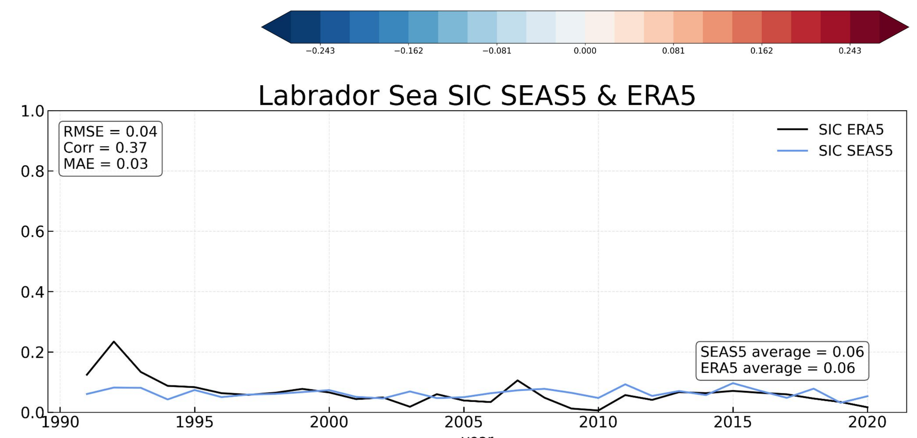

Figure (16): DJF Labrador Sea sea ice concentration 1991-2020 time series, for SEAS5 (blue) and ERA5 (black). Statistical metrics included in the inset boxes.

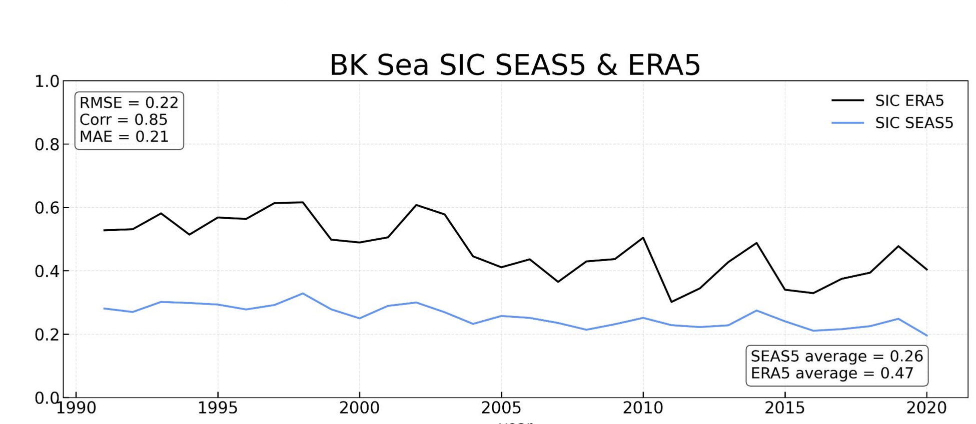

Figure (17): DJF Barents-Kara Sea sea ice concentration 1991-2020 time series, for SEAS5 (blue) and ERA5 (black). Statistical metrics included in the inset boxes.

WHAT'S NEXT?

- ➢ Add new diagnostics for the Atlantic Niño and the Southern Ocean.
- ➢ Combine all metrics in a scoreboard to characterise the global performance of the model in representing these key processes.
- ➢ Use this package to tune a seasonal forecast system based on IFS-NEMO-SI3 in the context of the PREDDYCT project.
- ➢ Make this Python-based package freely available to the scientific community.

References

- Acosta Navarro, J. C., Ortega, P., et al (2020). Link between autumnal Arctic sea ice and Northern Hemisphere winter forecast skill. *Geophysical Research Letters*, *47*(5), e2019GL086753.
- Dong, E., Song, F., et al (2025). The process-oriented understanding on the reduced double-ITCZ bias in the high-resolution CESM1. *Geophysical Research Letters*, *52*(1), e2024GL112087.
- Frigola, A., Martin-Martinez, E., et al(2025). The North Atlantic mean state in eddy-resolving coupled models: a multimodel study. *EGUsphere*, *2025*, 1-34.
- Kang, I. S., Kug, J. S., et al (2011). Impact of transient eddies on extratropical seasonal-mean predictability in DEMETER models. *Climate dynamics*, *37*(3), 509-519.
- O'Reilly, C. H. (2025). Signal-to-noise errors in early winter Euro-Atlantic predictions linked to weak ENSO teleconnections and pervasive jet biases. *Quarterly Journal of the Royal Meteorological Society*, e4952.
- Palmeiro, F. M., García-Serrano, J, et al (2023). Boreal winter stratospheric climatology in EC-EARTH: CMIP6 version. *Climate Dynamics*, *60*(3), 883-898